ELSEVIER

Geoderma 80 (1997) 417–429

GEODERMA

Observation of flow and transport processes in artificial porous media via magnetic resonance imaging in three dimensions

S. Oswald [a,*], W. Kinzelbach [a], A. Greiner [b], G. Brix [c]

[a] *Institute of Hydromechanics and Water Resources Management, ETH Zürich, ETH Hönggerberg, 8093 Zürich, Switzerland*

[b] *Institute of Environmental Physics, University of Heidelberg, INF 366, 69120 Heidelberg, Germany*

[c] *German Cancer Research Centre (DKFZ), Department of Radiological Diagnostic and Therapy, INF 280, 69120 Heidelberg, Germany*

Received 2 January 1997; accepted 27 March 1997

Abstract

In two series of laboratory experiments solute transport in saturated artificial porous media was observed using magnetic resonance imaging. The objective was to get qualitative and quantitative information on transport in three dimensions including heterogeneity effects and density driven convection phenomena. Characteristic finger growth rates were evaluated and compared to calculation results. The experiments show that magnetic resonance imaging measurements can be used successfully to clarify the role of heterogeneities in transport and to check the results of numerical calculations of density driven flow. © 1997 Elsevier Science B.V.

Keywords: groundwater; imaging; heterogeneity; dual porosity; transport; buoyancy; saltwater

1. Introduction

The difficulties encountered in the evaluation of transport processes in groundwater are mainly due to the poor accessibility of spatial information in

* Corresponding author. Tel.: +41 (0)1 6333142; Fax: +41 (0)1 6331061.

PII S0016-7061(97)00064-5

aquifers. Usually there are only some very localized measurements available in the places where boreholes exist. The problem is aggravated by the unknown heterogeneity of natural porous media. By tracer tests between boreholes it is possible to get some information, but this information is of an integrative nature.

In the laboratory spatial flow and concentration data are much better accessible than in the field. Lab studies are therefore more suited for the validation of numerical models and for the investigation into many basic concepts. Here experimental conditions are well controllable and characteristic properties can be predetermined to meet the conceptual assumptions to a high degree.

The advantages of lab studies can be further increased by using the technique of Magnetic Resonance Imaging (MRI). MRI represents a measurement method capable of noninvasively obtaining information on soil properties and flow and transport data in high resolution over the whole transport domain. Hence, with improving technical possibilities this technique is increasingly applied to flow problems in porous media. An overview of the corresponding MRI principles is presented by Van As and van Dusschoten (1997).

Generally there are two ways of applying this method in saturated media. One possibility is to visualize tracer transport using contrast agents or even enhanced tracers and analyse signal contrasts or even concentration values as was done by Guillot et al. (1991) to determine tracer dispersion or Pearl et al. (1993) to study convection and fingering driven by density forces in a box model. Another possibility is to measure velocities of fluid flow via special MRI techniques (Callaghan, 1991; Guilfoyle et al., 1992; Mansfield and Issa, 1994, 1996). This type of method has been applied e.g. on hydrodynamic dispersion (Seymour and Callaghan, 1996), diffusion (Snaar and Van As, 1993) and also on density-driven flow phenomena, namely thermal convection in a shallow cylindrical container (Shattuck et al., 1995).

To apply MRI on transport in heterogeneous porous media could strongly improve our understanding of the relevant mechanisms. Amin et al. (1993) studied the time-varying spatial distribution of water in dual porous soils. Hoffmann et al. (1996) prepared a horizontal saturated column with sand of different grain size and observed tracer transport through the column using high tracer concentrations, i.e. high signal contrast. The existence of preferential flow paths and their influence on water flow and tracer transport were clearly shown. Further measurements indicated that even small differences in fluid density can give rise to buoyancy effects and cause a rather different flow pattern.

Our study aimed towards the visualization of flow and transport in 3D in a porous medium with built-in heterogeneities of known characteristics and the observation of density driven flow. Low concentrations of a paramagnetic tracer were used which allowed the determination of tracer concentrations over the range of an order of magnitude.

2. Materials and methods

2.1. Comparison of transport in a homogeneous versus a heterogeneous soil column

The first set-up consisted of a vertical column (inner diameter 190 mm, length 282 mm) which was filled with a homogeneous porous medium built of silica glass beads (average diameter 0.5 mm, permeability of $1.9 \cdot 10^{-10}$ m^2). The beads were washed and oven-dried and the medium was saturated with deionized and degassed water. A pulse of water containing $CuSO_4$ as a tracer (8 mmol/l, total tracer mass 1.72 mmol) was pumped through the column via nineteen inlet openings at the bottom and one central outlet at the top. It was possible to interrupt the flow during the imaging periods, as molecular diffusion of the tracer is on this time scale negligible. The tracer concentration was also measured at the outlet using atomic absorption spectroscopy.

Besides the experiment in the homogeneous medium an experiment in a heterogeneous medium was performed. It contained 25 aggregates of lower permeability ($k = 0.8 \cdot 10^{-10}$ m^2), which had the shape of a pillow (about 34 mm $\times$ 39 mm in width, 13 mm in height) and were built into the homogeneous bead packing at five different heights in layers of five as described by Greiner (1995) in more detail.

2.2. Visualization of saltwater fingering developing in a situation of unstable density layering

In a second set-up the flow pattern induced by an unstable layering of saltwater above freshwater was observed via MRI as was done by Pearl et al. (1993) before in a smaller set-up. In this particular case no external flow was applied and the flow was entirely driven by density effects. A cubic container with 240 mm side length was filled with silica glass beads (average diameter 0.5 mm) and a cuboid zone with larger glass beads (average diameter 1.2 mm) was added in the centre (Fig. 1). The extension of this zone was 40 mm in each horizontal direction and 160 mm in the vertical direction. Its permeability, calculated via the Kozeny–Carman equation, was $1.0 \cdot 10^{-9}$ m^2, which is about five times higher than permeability in the surrounding medium. The permeability ratio was decreased to about 3 in a second experiment by increasing the size of the beads in the surrounding outer part to 0.7 mm average diameter.

The salt solution of 3 g/l in the upper part of the saturated packing in both experiments contained NaCl in a concentration of 2.04 g/l and the paramagnetic tracer $CuSO_4$ in a concentration of 0.96 g/l or 6 mmol/l. For these low concentrations the driving forces for flow, and hence flow velocities, are small enough to make 3D imaging possible. By cautiously removing the plastic sheet,

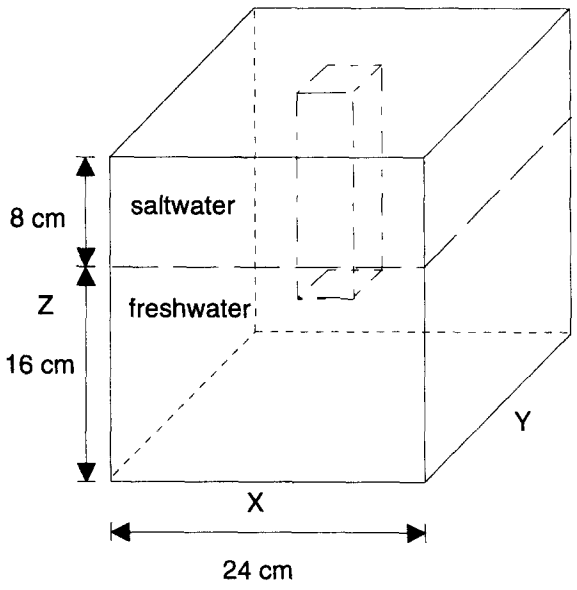

Fig. 1. Set-up of fingering experiment starting with a saltwater layer above freshwater.

initially separating the denser saltwater from the freshwater below, the convection process was started.

For both set-ups porosities were determined gravimetrically while permeabilities were calculated using the Kozeny–Carman equation.

2.3. Magnetic resonance imaging procedure

The experiments were carried out on a 1.5 tesla wholebody MRI system (Magnetom SP 63/84, Siemens, Erlangen, Germany) built for medical purposes. The standard body coil was used for all measurements, except that calibration measurements were performed using the standard headcoil due do the better signal-to-noise ratio of the acquired images.

MR images (matrix size, MA = 128 · 128; field of view, FOV = 300 mm) were acquired from 19 adjacent slices (thickness TH = 5 mm) in vertical direction using a two-dimensional spin–echo sequence (repetition time, T_R = 300 ms; echo time, T_E = 15 ms; number of excitations, N_{EX} = 2) before and after the administration of paramagnetic copper sulphate as tracer (Greiner et al., 1997). For the actual values of the spin–lattice relaxation time T_1 and spin–spin relaxation time T_2 this denotes a T_1-weighted type of measurement. The tracer behaviour was observed over a period of up to 3 h with a temporal resolution of about 3 min.

In case of the vertical flow column set-up the parameters were basically identical, except that 24 slices (TH = 10 mm) were measured parallel to the

flow direction, thus scanning the entire column, and T_R was chosen to be 120 ms instead of 300 ms.

The signal intensity S in a particular volume element for this type of measurement is dependent on the NMR measurement and physical parameters according to (Krestel, 1988; Guillot et al., 1991; Brix, 1992; Hoffmann et al., 1996)

$$S \propto \rho_P \exp\left(-\frac{T_E}{T_2}\right)\left\{1-\exp\left(-\frac{T_R}{T_1}\right)\right\} \tag{1}$$

where ρ_P is proportional to the proton density.

The spin–lattice relaxation time T_1^0 of pure water in the porous medium is reduced due to surface relaxation at the porous matrix. In an artificial porous medium like the homogeneous bead packings used, the magnetization decay can be assumed to be mono-exponential, because the distribution of pore sizes is very narrow (Kleinberg et al., 1994).

Additionally, T_1 is further reduced due to dipolar interactions between protons and paramagnetic ions (Nierendorf and Haustein, 1992; Carrington and McLachlan, 1979)

$$\frac{1}{T_1} = \frac{1}{T_1^0} + \beta \cdot C \tag{2}$$

where β accordingly denotes the relaxivity and c the concentration.

If the grain size of the porous matrix or the pore size, respectively, are small, then the spin–spin relaxation time T_2 is reduced significantly because of diffusion of water molecules in the field gradients around the grains. Paramagnetic ions that are present in reasonably low concentrations will further reduce T_2, but not significantly.

The relative signal enhancement caused by the tracer

$$S_{rel} = \frac{S(c) - S(c=0)}{S(c=0)} \tag{3}$$

is computed pixel-by-pixel. For the grain sizes used, the range of concentrations and the repetition and echo times have been chosen in such a manner, that the relation between the relative signals and the tracer concentration was in a very good approximation linear. This was observed to be true at least within the range from 1 mmol/l to 10 mmol/l (Fig. 2).

Ranges of approximately linear behaviour are similarly observed for other paramagnetic tracer ions such as Mn^{2+} (Guillot et al., 1991) or Ni^{2+} (Pearl et al., 1991). This linear relationship has the advantage that solute concentrations can be deduced from the measured signal in a simple way and over a reasonable range of concentrations. In general large concentrations of other ions present,

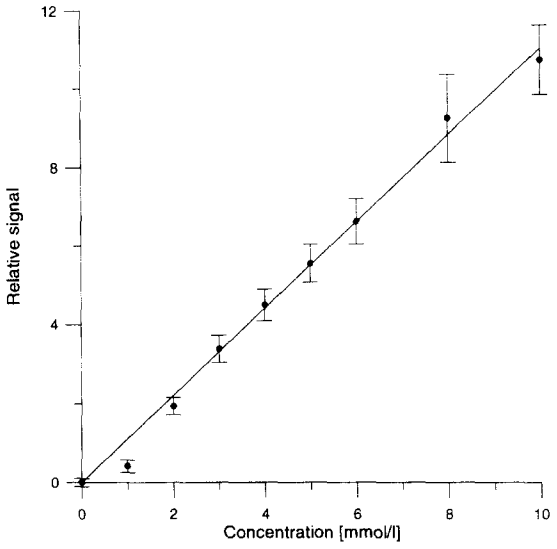

Fig. 2. Measured relative signal amplitudes of samples containing tracered water in a bead packing for calibration. A linear fit was used to obtain concentration values over the total range (Greiner et al., 1997).

e.g. sodium chloride, could affect the signal amplitude and have to be considered in calibration.

To eliminate signal variations over the examined FOV due to the porous nature of the phantom and inhomogeneities in the sensitivity of the coil, proton-density weighted spin–echo images ($T_R = 8000$ ms; $T_E = 15$ ms; $N_{EX} = 1$) were also measured. For the flow column set-up these data were used to improve the quality of the calibration by normalizing signals with the signal intensity of the density-weighted images as described by Greiner et al. (1997).

Due to the particular preparation method of the fingering set-up the upper part of the phantom contained tracer from the beginning and hence no full image without tracer influence could be obtained. In this case, the proton-density weighted measurements were used to get relative signals. Additionally, to improve spatial and temporal resolution only part of the container was scanned in these fingering experiments, and tracer concentration was measured in a vertical slab or horizontal slab, respectively. Hence each volume element still was an average over several glass beads and the corresponding pores.

3. Results and discussion

The evolution of concentration in time in a vertical cross-section of the homogeneous and the heterogeneous columns shown in Fig. 3 provides a good

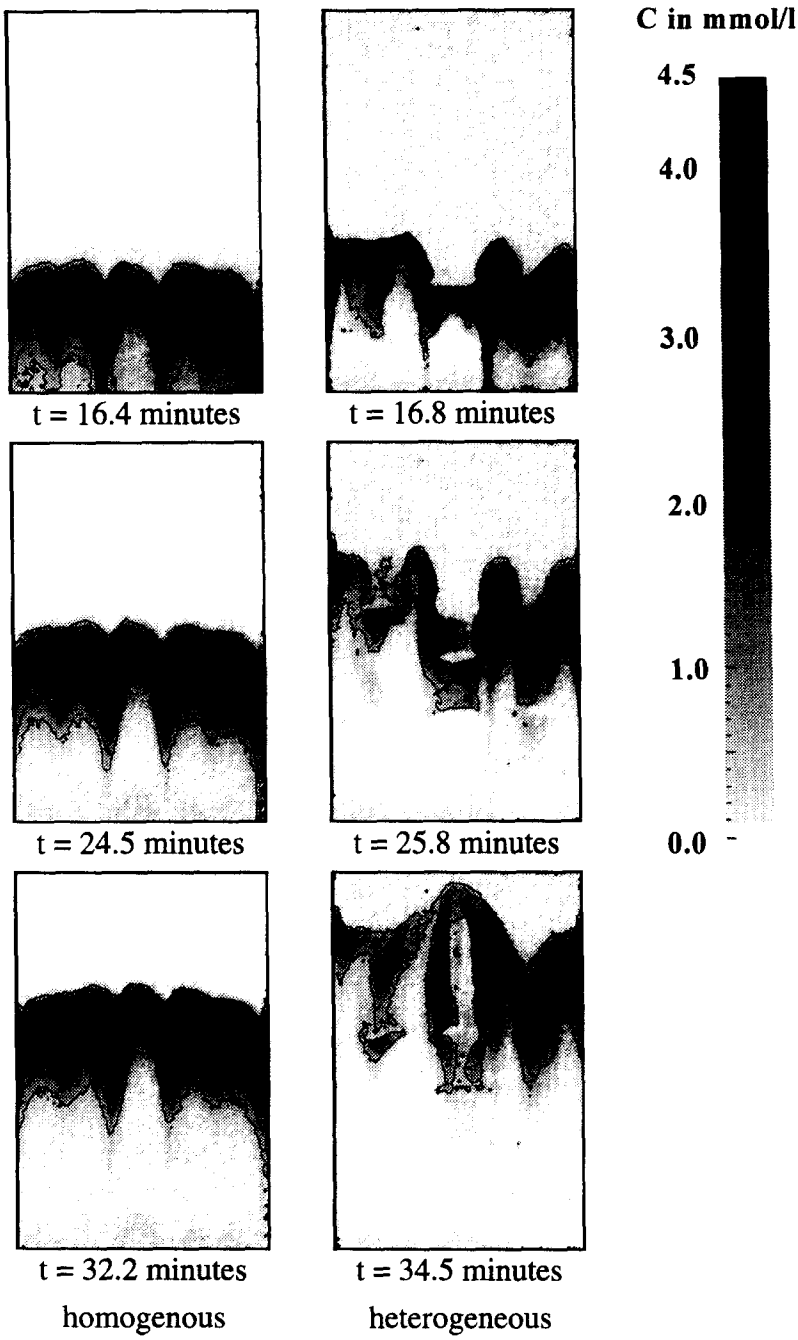

Fig. 3. Comparison of the tracer concentration evolution in a vertical cross-section. Left the homogeneous column, $Q = 61.2$ ml/min; right the heterogeneous column filled with aggregates of lower permeability, $Q = 62.3$ ml/min. Isolines are shown at 0.45, 0.9, 1.8, and 2.7 mmol/l.

proof of the differences in flow and transport between the two set-ups. Openings strongly influence the homogeneity of the flow and concentration distribution, even when inflow was distributed over a large number of inlet openings.

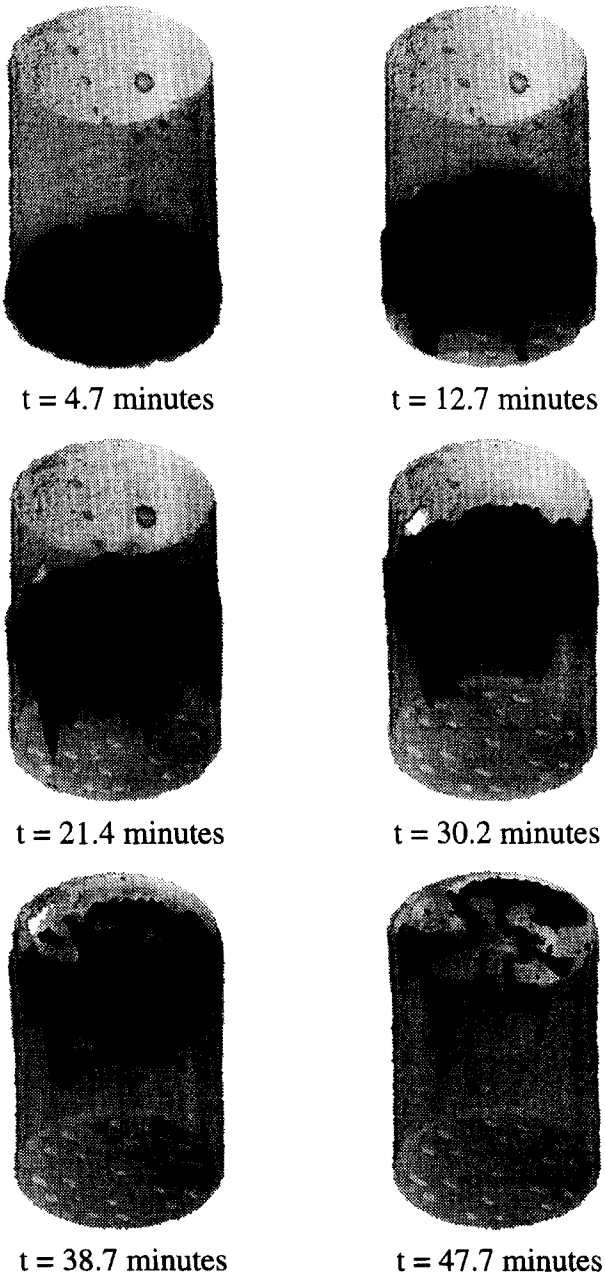

Fig. 4. Propagation of the isosurface of 25% of the maximum tracer concentration through the heterogeneous column.

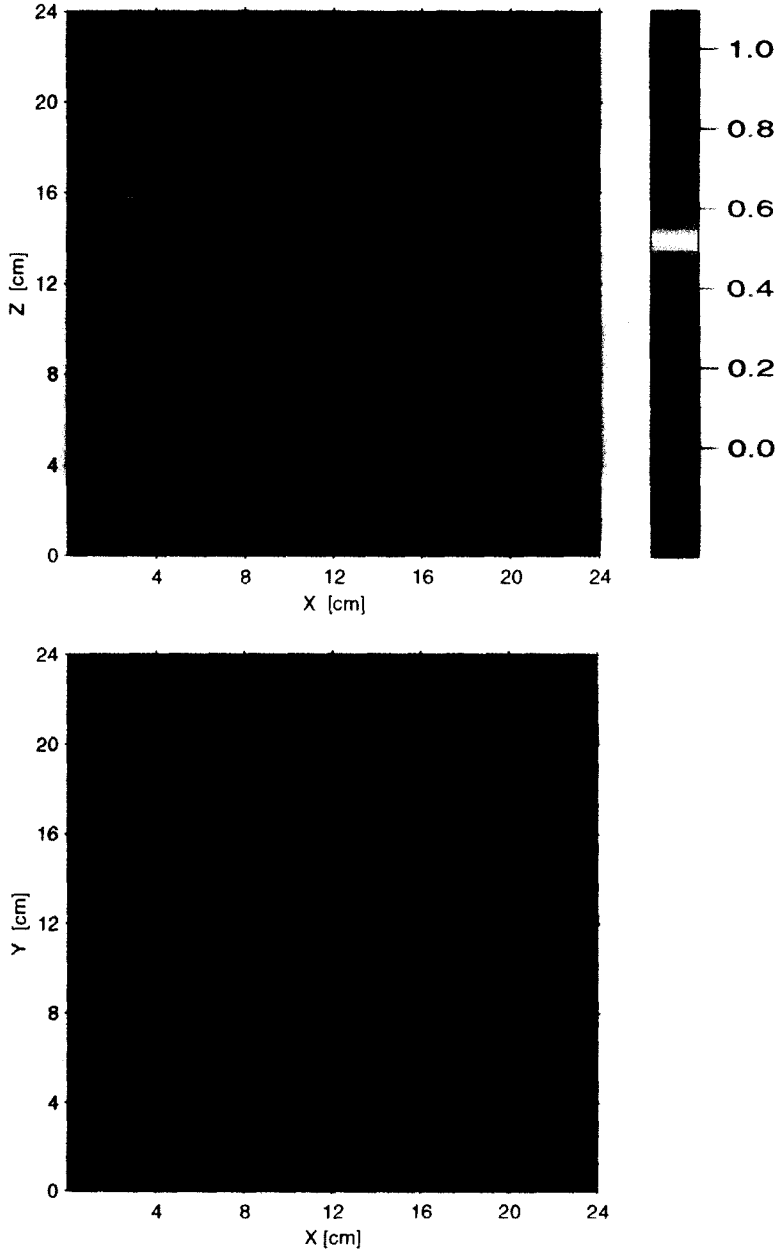

Fig. 5. Fingering of saltwater in unstable layering with central heterogeneity, relative concentrations after subtraction of a mean freshwater signal level. (a) Vertical centre plane, permeability ratio of 5.1, after 176 min. (b) Horizontal plane, permeability ratio of 3.2, 4 cm below initial interface, after 166 min.

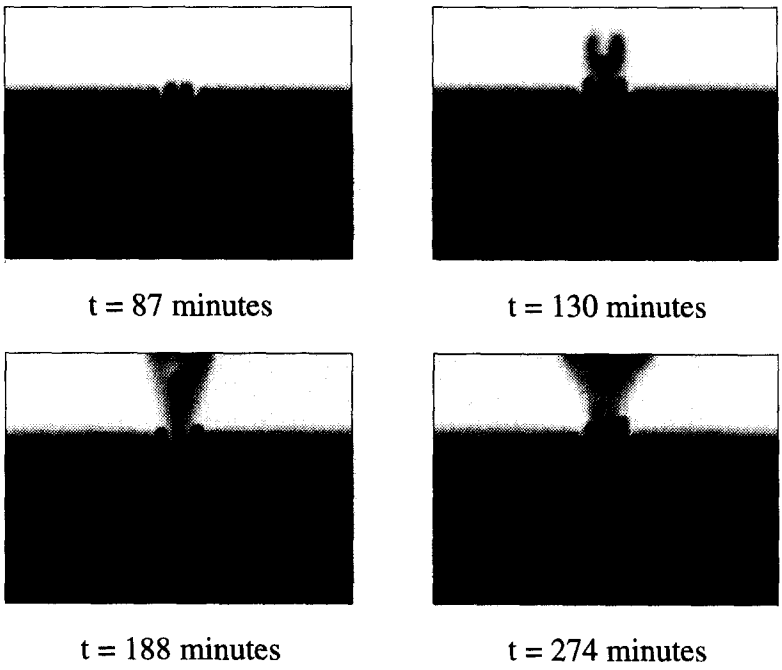

Fig. 6. Vertical diagonal cross-section through the fingering experiment model allowing the determination of the growth rate of the main saltwater fingers.

Regardless of this shortcoming the significant change in transport of tracer due to the aggregates of lower permeability is obvious. This leads to an increase in dispersion of the tracer front and also a net retardation compared to the homogeneous column flow. It is important to notice that for identical discharge Q the tracer front in the case of low-permeability heterogeneities is moving faster than in the homogeneous case due to the smaller amount of mobile porosity available for the main flow.

The three-dimensional plot of a concentration isosurface (Fig. 4) confirms this result and gives an even better view of the tracer propagation.

The mass balances achieved were reasonably accurate and in good agreement with the concentration determination at the outlet. Additionally, by using the MRI data transport constants like dispersivities could be evaluated and compared with other measurements or with calculations. Distortions e.g. caused by non-parallel flow fields close to inlet and outlet or by unexpected heterogeneities could be eliminated much better than if breakthrough curves had been measured only.

In the second type of experiment the advective fingering of saltwater occurred from the beginning simultaneously with mixing by diffusion. The fingering started first in the zone of higher permeability, where the degree of instability as for example expressed by a Rayleigh number is largest, then fingers developed

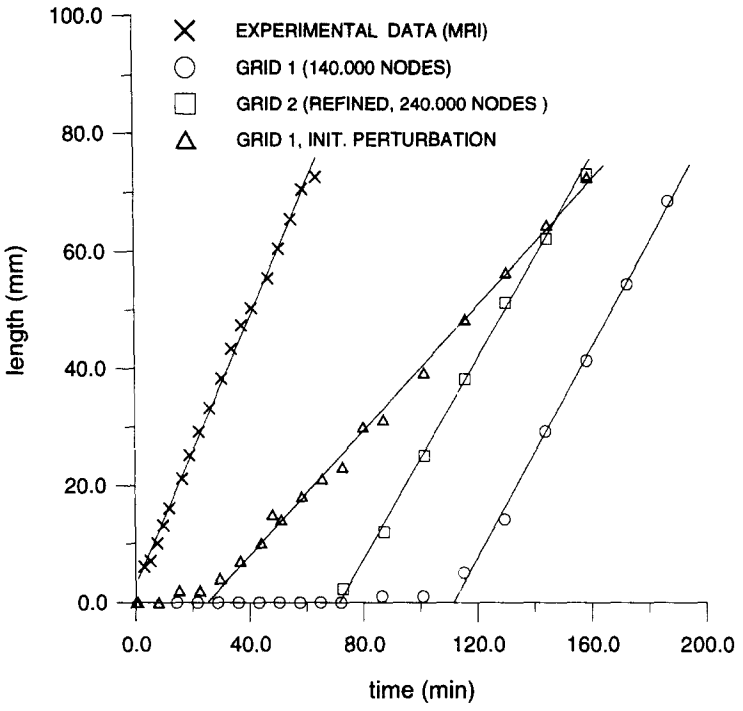

Fig. 7. Comparison of calculated and measured finger growth speeds. The simulated fingers can reproduce the correct growth rate, but their onset is delayed.

also in the zone of lower permeability (Fig. 5). The saltwater fingers in the centre coalesce and pool when reaching the end of the zone of higher permeability.

The obtained data were used to test the capabilities of the numerical code SALTFLOW (Frind and Molson, 1994). The numerical simulation of the experiments (Oswald et al., 1996) cannot be compared with the experimental MRI data point by point due to the unstable nature of the phenomenon which leads to a non-unique concentration distribution. Therefore, more generic flow properties such as finger growth speed or finger size should be evaluated from experimental and simulated data (Fig. 6).

In the simulation the start of the fingers was always delayed compared to the MRI data. This delay is shortened if the numerical grid is refined. In both cases the finger growth rate of the experimental data could be reproduced well (Fig. 7). Another simulation including some initial perturbation shortened the delay but reduced the finger growth speed and hence was not capable to simulate the effect of the real perturbations responsible for finger initialization nor to neutralize numerical suppression of the onset of fingering. All simulations failed to show the fingering observed in the low-permeability area.

The main difficulties encountered in the set-up and the preparation of the experiment were to create the intended boundary and initial conditions, to find glass beads with chemical properties suited to avoid signal artefacts in the images, and to prevent air-bubbles from forming in the porous medium. The problems with air bubbles occur mainly in the fingering experiment, because the removal of the plastic sheet tended to cause air-bubbles, and also other perturbations of the horizontal interface between saltwater and freshwater. On the other hand, the MRI itself yields valuable information about the properties of the scanned volume and its boundary conditions. For example, the structure of the flow field at the inflow and outflow regions could be observed in the case of the vertical flow column. This allowed an improved determination of the dispersion coefficients (Greiner, 1997).

The capability of the MRI method to determine concentration values in a porous medium is restricted to a range of concentrations close to the maximum concentration used, because the signal amplitude of the freshwater regions itself is about 10% of the maximum signal amplitude and because it also varies over the scanned volume. This is primarily due to the fact, that the percentage of fluid in the voxels is not spatially constant, since each voxel contains in some cases less than 20 beads thus still allowing statistical variations. The normalization of the signal can not fully compensate for the spatial variations of the signal amplitude due to the built-in heterogeneities and field inhomogeneities.

4. Conclusions

Imaging with NMR can be a very beneficial tool in getting a better understanding of the flow and transport processes taking place in soils. Characteristic properties of the porous media used can be checked and transport parameters can be evaluated in a more meaningful way which avoids lumping of systematic disturbances (e.g. by heterogeneities or imperfect boundary conditions) into a dispersivity for example.

A growing demand of high resolution three-dimensional and time-dependent data exists especially in order to check the reliability of both model formulations, numerical codes, and discretization requirements. In this field MRI can make a valuable contribution.

References

Amin, M.H.G., Chorley, R.J., Richards, K.S., Bache, B.W., Hall, L.D., Carpenter, T.A., 1993. Spatial and temporal mapping of water in soil by magnetic resonance imaging. Hydrol. Process. 7, 279–286.

Brix, G., 1992. Grundlagen der MRT und MRS—Physikalische Grundlagen. In: Reisser, M., Semmler, W. (Eds.), Magnetresonanztomographie. Springer-Verlag, Berlin, pp. 40–44.

Callaghan, P.T., 1991. Principles of Nuclear Magnetic Resonance Microscopy. Clarendon Press, Oxford.

Carrington, A., McLachlan, A.D., 1979. Introduction to Magnetic Resonance. Chapman and Hall, London.

Frind, E., Molson, J., 1994. SALTFLOW 2.0 user guide. Waterloo Centre for Groundwater Research, University of Waterloo, Canada.

Greiner, A., 1995. Visualisierung von Transport in porösen Medien mithilfe von MR-Tomographie. Diploma Thesis, University of Heidelberg.

Greiner, A., Schreiber, W., Brix, G., Kinzelbach, W., 1997. Magnetic resonance imaging of paramagnetic tracers in porous media: quantification of flow and transport parameters. Water Resour. Res. 33 (6), 1461–1473.

Guilfoyle, D.N., Mansfield, P., Packer, K.J., 1992. Fluid flow measurement in porous media by echo-planar imaging. J. Magn. Reson. 97, 342–358.

Guillot, G., Kassab, G., Hulin, J.P., Rigord, P., 1991. Monitoring of tracer dispersion in porous media by NMR imaging. J. Phys. D, Appl. Phys. 24, 763–773.

Hoffmann, F., Ronen, D., Pearl, Z., 1996. Evaluation of flow characteristics of a sand column using magnetic resonance imaging. J. Contam. Hydrol. 22, 95–107.

Kleinberg, R.L., Kenyon, W.E., Mitra, P.P., 1994. Mechanism of NMR relaxation of fluids in rock. J. Magn. Reson., Ser. A 108, 206–214.

Krestel, E. (Ed.), 1988. Bildgebende Systeme für die medizinische Diagnostik. Siemens Aktiengesellschaft, Berlin.

Mansfield, P., Issa, B., 1994. Studies of fluid in porous rocks by echo-planar MRI. Magn. Reson. Imaging 12 (2), 275–278.

Mansfield, P., Issa, B., 1996. Fluid transport in porous rocks. 1. Epi studies and a stochastic model of flow. J. Magn. Reson., Ser. A 122, 137–148.

Nierendorf, H.P., Haustein, J., 1992. Grundlagen der MRT und MRS—Kontrastmittel. In: Reisser, M., Semmler, W. (Eds.), Magnetresonanztomographie. Springer-Verlag, Berlin, pp. 83–85.

Oswald, S., Schwarz, C., Kinzelbach, W., 1996. Benchmarking in numerical modelling of density driven flow. Proc. of 14th Salt Water Intrusion Meeting SWIM 96, Rep. 87, Geological Survey of Sweden, Uppsala, pp. 32–40.

Pearl, Z., Magaritz, M., Bendel, P., 1991. Measuring diffusion coefficients of solutes in porous media by NMR imaging. J. Magn. Reson. 95, 597–602.

Pearl, Z., Magaritz, M., Bendel, P., 1993. Nuclear magnetic resonance imaging of miscible fingering in porous media. Transport in Porous Media 12, 107–123.

Seymour, J.D., Callaghan, P.T., 1996. 'Flow-diffraction' structural characterization and measurement of hydrodynamic dispersion in porous media by PGSE NMR. J. Magn. Reson., Ser. A 122, 90–93.

Shattuck, M.D., Behringer, R.P., Johnson, G.A., Georgiadis, J.G., 1995. Onset and stability of convection in porous media: visualization by magnetic resonance imaging. Phys. Rev. Lett. 75 (10), 1934–1937.

Snaar, J.E.M., Van As, H., 1993. NMR self-diffusion measurements in a bounded system with loss of magnetization at the walls. J. Magn. Reson., Ser. A 102, 318–326.

Van As, H., van Dusschoten, D., 1997. NMR imaging of transport processes in micro-porous systems. In: Hemminga, M.A., Buurman, P. (Eds.), NMR in Soil Science. Geoderma 80 (3/4), 389–403, this issue.